A Molecular Mechanics Force Field for Biologically Important Sterols

ZOE COURNIA,[1] JEREMY C. SMITH,[1] G. MATTHIAS ULLMANN[1,2]
[1]*Computational Molecular Biophysics, Interdisciplinary Center for Scientific Computing (IWR), Im Neuenheimer Feld 368, Universität Heidelberg, 69120 Heidelberg, Germany*
[2]*Structural Biology and Bioinformatics; Bayreuth Center of Molecular Biosciences, Universität Bayreuth, Universitätsstr. 30, BGI, 95447 Bayreuth, Germany*

Received 18 March 2005; Accepted 24 May 2005
DOI 10.1002/jcc.20277
Published online in Wiley InterScience (www.interscience.wiley.com).

Abstract: A parameterization has been performed of the biologically important sterols cholesterol, ergosterol, and lanosterol for the CHARMM27 all-atom molecular mechanics force field. An automated parameterization method was used that involves fitting the potential to vibrational frequencies and eigenvectors derived from quantum-chemical calculations. The partial charges were derived by fitting point charges to quantum-chemically calculated electrostatic potentials. To model the dynamics of the hydroxyl groups of the sterols correctly, the parameter set was refined to reproduce the energy barrier for the rotation of the hydroxyl group around the carbon connected to the hydroxyl of each sterol. The frequency-matching plots show good agreement between the CHARMM and quantum chemical normal modes. The parameters are tested in a molecular dynamics simulation of the cholesterol crystal structure. The experimental geometry and cell dimensions are well reproduced. The force field derived here is also useful for simulating other sterols such as the phytosterols sigmasterol, and campesterol, and a variety of steroids.

 J Comput Chem 26: 1383–1399, 2005

Key words: cholesterol; ergosterol; lanosterol; force-field parametrization; biomembranes; CHARMM

Introduction

Cholesterol performs a wide range of roles in human cells. It is the precursor for the synthesis of hormones and numerous other biologically important molecules.[1–3] Lipid membranes of eukaryotic cells have a complex composition consisting of hundreds of different lipids and proteins, plus cholesterol or closely related sterols. In mammalian cells, cholesterol has been found to account for up to 50% of the lipid concentration in the plasma membrane. The effect of cholesterol and other biologically important sterols, such as lanosterol and ergosterol, on functional, structural, and dynamical membrane properties has received considerable attention in the past decades. Cholesterol has been shown to influence the physical properties of membranes, such as regulating their fluidity,[4,5] and may also play other roles, such as in signal transduction[6] and ion permeation.[7] Ergosterol (provitamin D_2) can be found in the membranes of fungi, yeasts, and protozoans. Lanosterol, the evolutionary and biosynthetic precursor of cholesterol,[8] is the major constituent of prokaryotic cell membranes.

Cholesterol, ergosterol, and lanosterol have very similar chemical structures (Fig. 1a, b, and e, respectively). However, they exert different influences on membrane properties.[5,9] Cholesterol has a saturated side chain, while ergosterol has a *trans* double bond at position C_{22} and lanosterol a double bond at position C_{24}. The main structural difference of lanosterol from the other two sterols is the presence of three extra methyl groups (two at position C_4 and one at C_{14}) that protrude from its otherwise flat surface. In the steroid ring system cholesterol has a double bond between carbons C_5 and C_6, in contrast to lanosterol's double bond between C_8 and C_9. Ergosterol, on the other hand, has a conjugated π-system in its second steroid ring which has two *cis* hydrogens on positions C_6 and C_7. These subtle structural differences seem to have a strong effect on membrane structure and dynamics, and therefore accurate representation of the structure and dynamics of these molecules is required for useful simulation studies of their properties. Although ergosterol and lanosterol are structurally very similar to cholesterol, only cholesterol has been chosen by evolution to be the

Correspondence to: M. Ullmann; e-mail: Matthias.Ullmann@uni-bayreuth.de

Contract/grant sponsor: BMBF; Contract/grant number: 03SHE2HD

This article includes Supplementary Material available from the authors upon request or via the Internet at http://www.interscience.wiley.com/jpages/0192-8651/suppmat

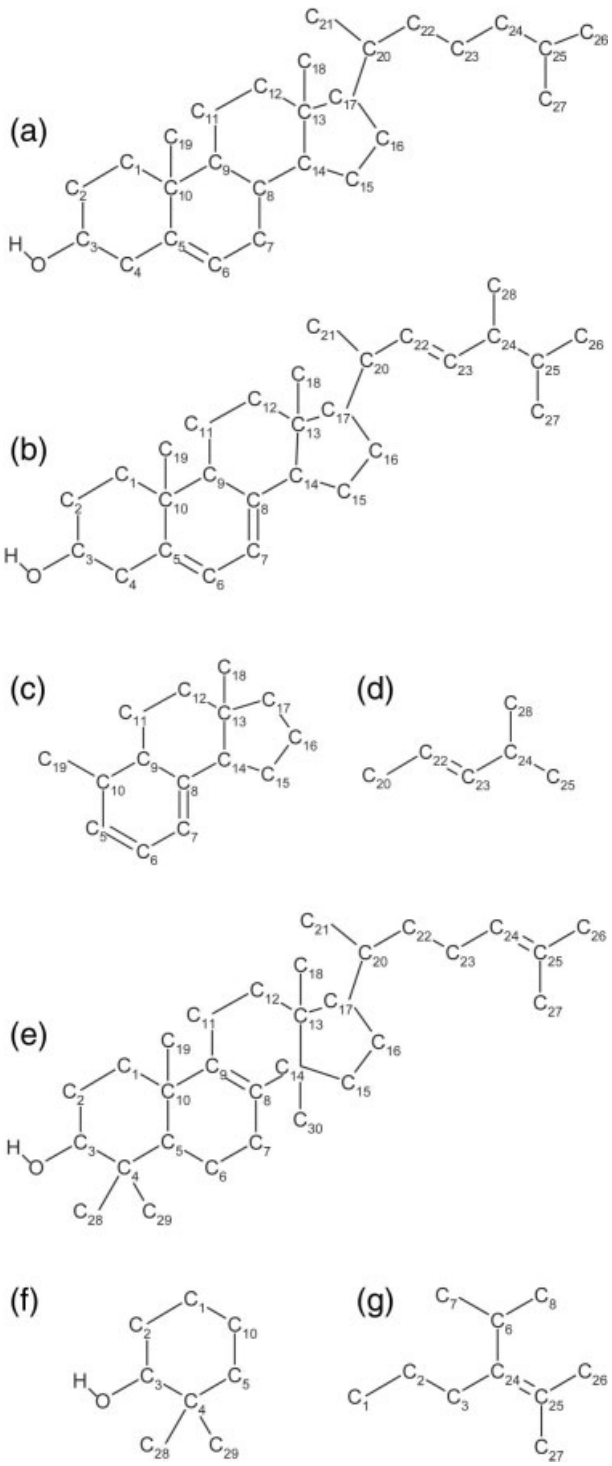

Figure 1. The atom numbering scheme of (a) cholesterol, (b) ergosterol, (c) NP, (d) 4-methyl-pent-2-ene, (e) lanosterol, (f) 2,2-dimethyl cyclohexanol, (g) 3-isopropyl-2-methylhex-2-ene.

major constituent of the mammalian plasma membranes. Moreover, the process of conversion of lanosterol to cholesterol in mammalian cells is laborious, requiring 18 enzymatic steps.[8] Therefore, an intriguing question concerns what the particular characteristics of cholesterol are, which have led to its evolutionary selection in mammalian plasma membranes, given the presence of structurally very similar precursors. One clue may be that, in contrast to the analogs, cholesterol has been shown to reduce membrane permeability and to increase ordering of the phospholipids.[10] Moreover, cholesterol dramatically influences the gel–liquid crystal phase transition of phospholipids by introducing a new thermodynamically stable region of coexistence between the liquid and crystal phase: the liquid-ordered (lo) phase.[11–13]

The physical properties of mammalian plasma membranes can be reproduced and studied with model biological membranes.[1] Experimental and computational studies of the model systems have been used to shed light on the nature of membrane-sterol interactions. Experimental studies aimed at determining how cholesterol influences membrane properties very often lack sufficient resolution for investigating the underlying molecular interactions that drive the observed properties. In contrast, using molecular dynamics (MD) simulation, it is possible to interpret experimental results on complex membrane systems in detail and to gain insight into the relevant interactions at the atomic level. The field of lipid bilayer simulations is growing rapidly and the level of complexity of the systems treated is increasing, with explicit inclusion of membrane proteins[14–17] and cholesterol[9,18–20] in the simulated systems.

The functional form of the force field used in an MD simulation must be used in conjunction with a set of empirical parameters that are molecule dependent and must be optimized prior to performing simulations. This optimization step is generally referred to as parametrization of the force field. The reliability of a molecular mechanics calculation is dependent on both the functional form of the force field and on the numerical values of the associated parameters. Thus, the first necessary step towards a reliable MD simulation is the parametrization procedure. Most "all-atom" empirical force fields used in common MD packages (such as CHARMM[21]) are equipped with parameter sets for modeling and combining the basic building blocks of biomolecules, but often not for more exotic molecules such as steroids or sterols.

In the literature, two force field studies on cholesterol have appeared, for the CFF93[22] and CVFF[23] force fields,[24] and for GROMOS96.[25,26] The first study reproduces quite accurately the crystal structures of anhydrous cholesterol[27] and cholesterol acetate,[28] and examines further the rigidity of the tetracyclic ring of cholesterol and cholesterol–cholesterol interactions. The latter study tested the existing GROMOS 96 force field against the cholesterol hemiethanolate crystal.[29] Although the poor quality of the crystal is a limiting factor for the results, the force field adequately reproduces the crystal properties; problems observed in this study with the conformation of the alkyl chain might arise from the united atom approximation used. Most of the recently reported cholesterol:membrane simulations have used united atom models.[9,18,30] Although united-atom force fields are rapid to calculate, all-atom force fields may be required for the accurate modelling of some cholesterol:lipid interactions or the simulation of experimental techniques that probe hydrogen–atom dynamics, such as nuclear magnetic resonance (NMR) or incoherent neutron scattering.

In the present study, we present a new parameter set for cholesterol, ergosterol, and lanosterol for the CHARMM force field. The work involved refining a preliminary parameter set for cholesterol[31] and developing from scratch sets for ergosterol and lanosterol. The parameters are obtained using the Automated Frequency Matching Method (AFMM),[32,33] an efficient automated way of generating intramolecular force field parameters based on quantum chemical normal modes. Furthermore, care has been taken to reproduce the results for important rotational energy barriers. The final refined set for cholesterol is tested on the available crystal structure.[27]

Methods

Computational Details

All quantum chemical calculations were performed with the NWChem 4.5 package.[34] Geometry optimizations and normal mode analyses were performed at the DFT/B3LYP level of theory and with the Stevens–Basch–Krauss–Jasien–Cundari[35] (SBKJC) basis set for the isolated molecules. To reduce computational time, the effective core potential (ECP) of SBKJC was used for the carbons and the oxygen. ECPs replace the core electrons with an effective potential, thus eliminating the need for calculating the core basis functions, which usually require a large set of Gaussians to describe them. Geometry optimizations were performed to a maximum gradient of 0.00045 a.u. and a root-mean-square gradient of 0.0003 a.u. in the Cartesian coordinates. The frequencies were calculated numerically. A frequency scaling factor of 0.9614 was used to compensate for the use of the harmonic approximation to the potential energy surface (http://srdata.nist.gov/ccbdb; National Institute of Standards and Technology).[36] For the calculation of partial atomic charges, all the structures were first optimized at the DFT/6-31G(d) level of theory, and then the CHELPG method[37] in NWChem was used to derive them.

The CHELPG method employs a least-squares fitting procedure to determine the set of atomic partial charges that best reproduces the quantum mechanical electrostatic potential at selected grid points. The grid was extended to 3 Å from any of the atomic centers and the grid spacing was set to 0.1 Å. The grid points for which the QM electrostatic potential was evaluated and used in the fitting procedure of the partial atomic charges, all lie outside the van der Waals radii of the atoms and within a cutoff distance from the atomic centers. In this study, all grid points lying within a distance less than 2 Å from any of the atomic centers were discarded.

The fitting was subjected to the constraint that the sum of the charges should be equal to the net charge on the molecule. To ensure that the charges on symmetrically equivalent atoms are equal, additional constraints on the partial atomic charges were imposed during the fitting procedure. In particular, the molecule was grouped into subsets of atoms, which were each constrained to have zero total charge. For example, the methyl groups were restrained to zero charge with, in addition, all the hydrogens carrying identical charges. The Hartree–Fock (HF) method was not preferred for the calculation of the charges, as it has been shown that HF/6-31G* RESP charges systematically overestimate dipole moments.[38] This overestimation may be tolerable when the system studied is solvated in a polar solvent, as the overestimated charges implicitly incorporate polarization effects on the molecular charge distribution. However, in an apolar environment such as a lipid bilayer, overestimation of the partial charges is not desired.

All molecular mechanics calculations were performed using the CHARMM27 package.[21] Except for the new parameters, which are derived here, the existing CHARMM atom-type parameters were used.[39–42] The molecular mechanics minimizations were carried out using the Steepest Descent algorithm for initial minimization, followed by Newton–Raphson minimization with a convergence criterion for the energy gradient of 10^{-6} kcal/mol/Å. Nonbonded interactions were cutoff at 12 Å using the CHARMM shifted potential.[21]

In CHARMM, the empirical potential energy function is given by eq. (1):

$$V(\mathbf{r}^N) = \sum_{\text{bonds}} K_b(b - b_0)^2 + \sum_{ub} K_{ub}(s - s_0)^2 + \sum_{\text{angles}} K_\theta(\theta - \theta_0)^2 + \sum_{\text{dihedrals}} K_\chi(1 + \cos(n\chi - \chi_0)) + \sum_{\text{impropers}} K\psi(\psi - \psi_0)^2 + \sum_{\text{nonbond}} \varepsilon_{ij}\left[\left(\frac{R_{ij}^{\min}}{r_{ij}}\right)^{12} - \left(\frac{R_{ij}^{\min}}{r_{ij}}\right)^{6}\right] + \frac{q_i q_j}{D r_{ij}} \quad (1)$$

where K_b, K_{ub}, K_θ, K_ϕ are, respectively, the bond, Urey–Bradley, angle, dihedral, and improper dihedral constants, and b, s, θ, χ, and ϕ represent, respectively, bond lengths, Urey–Bradley 1–3 distances, bond angles, dihedral angles, and improper torsion angles (the subscript zero is used to represent the corresponding equilibrium value). Nonbonded interactions between pairs of atoms (labeled i and j) at a relative distance r_{ij} are described by the Lennard–Jones 6–12 (LJ) term for the van der Waals interactions and the Coulomb interaction term for the electrostatics. $R_{ij}^{\min}$ and ε_{ij} are, respectively, the distance between atoms i and j at which the LJ potential is minimum and the depth of the LJ potential well for the same pair of atoms. In the article, the van der Waals energies always correspond to energies calculated with the LJ potential. D is the effective dielectric constant ($D = 1$ in the present case) and q_i the partial atomic charge on atom i.

MD simulation on the cholesterol crystal structure was performed at constant pressure–temperature with periodic boundary conditions and an integration timestep of 0.001 ps. Starting from experimental coordinates, and after minimization, the system was heated up to 500 K with 10-K temperature steps. Subsequently, the system was equilibrated for 10 ps using velocity rescaling followed by a second phase of equilibration without velocity rescaling for 10 ps at 298 K (the experimental temperature). Finally, production dynamics followed for 2 ns at 298 K.

Parameter Refinement

The values of the various parameters in eq. (1) must be determined. These parameters cannot be directly determined from experiments. The experimental data that pertain to force field calculations, such as infrared frequencies or crystal lattice constants are not a simple function of the force field parameters. Force field

parameters are more directly connected to quantities that are well-defined theoretically, such as the second derivatives of the energy with respect to coordinates (i.e., the Hessian matrix elements). These quantities can therefore be obtained via quantum chemical calculations.

Before refinement, an initial set of parameters must be determined. The LJ parameters ε_{ij} and R_{ij} depend mostly on atomic properties, and are relatively insensitive to changes in the molecular environment. Here, these were directly transferred from original CHARMM values and were not modified during refinement.

Equilibrium values for bonds b_0, angles σ_0, and dihedrals χ_0 that were not existing in the original CHARMM force field parameter file[39–42] were derived from the optimized quantum chemical structure and were not further optimized. An initial guess, based on analogy to similar existing CHARMM parameters and on chemical intuition, was made for all other missing parameters.

Equilibrium values and hybridization of the atoms involved should be carefully considered when deriving a set of initial parameters. In some cases it is necessary to derive initial parameters from rotational potential energy profiles (single-point QM energy calculations) before achieving good optimization. This approach is particularly useful for critical torsion parameters. Further, after designing the initial parameter set, one can match the MM normal modes with reference normal modes and by visual inspection to check the motions involved in any exchanged eigenvector modes, using the Molden program,[43] for example. This procedure can give a first hint as to which parameters were not appropriately designed or should be manually adjusted. The H–O–C_3–C_2 dihedral (see Fig. 1) was optimized by fitting the rotational energy barrier to the potential derived by quantum mechanical single-point calculations. These parameters were determined before the optimization and remained fixed during the rest of the optimization procedure.

The initial parameter set was used for minimization and calculation of normal modes (eigenvalues and eigenvectors) with CHARMM. The parameters were optimized by comparing the normal modes thus obtained with reference normal modes calculated with the quantum chemistry methods, by employing the AFMM method.[32] AFMM uses an iterative procedure to refine the parameters so as to reproduce the quantum-chemical reference set normal modes (both eigenvalues and eigenvectors).

An efficient way to check simultaneously for both orthonormality and frequency matching is to project each of the CHARMM eigenvectors onto the reference set of eigenvectors and to find the frequency $v_j^{\max}$ corresponding to the highest projection. Plotting this frequency against the corresponding frequency v_i, would in the ideal case, give a one-to-one relationship: $v_i = v_j^{\max}$. Points that deviate from the ideal plot may indicate exchanged or mismatched frequencies. AFMM is based on iteratively minimizing the sum-of-squares, Y^2 of the deviations from the ideal situation as follows:

$$Y^2 = \sum_{3N-6} (v_i - v_j^{\max})^2 \quad (2)$$

where N is the number of atoms in the molecule and there are $3N - 6$ independent vibrational frequencies.

The range over which parameters were allowed to vary was ± 300 kcal/mol/Å^2, ± 100 kcal/mol/rad^2, ± 5 kcal/mol, and ± 20 kcal/mol/rad^2 for the bond, angle, dihedral, and improper force constants, respectively. To check for convergence of the function Y^2, the optimizations were allowed to run until the value of Y^2 remained constant for at least 6000 steps. The root-mean-square deviation, σ, from the reference case is also calculated:

$$\sigma = \sqrt{\frac{\sum_{3N-6} (v_i - v_j^{\max})^2}{3N - 6}} \quad (3)$$

A desirable property of MM force fields is the transferability of the parameter set, that is, the possibility to transfer parameters from one molecule to another. In this respect, when designing a new parameter set addition of new atom types to the force field should be limited only to those specific cases in which existing types cannot be used. For the parameterization of cholesterol and lanosterol, it was not necessary to define any new atom types for CHARMM, and the parameterization was based on existing lipid atom types. For the sp^3 atoms the atom types used were CTL1, CTL2, and CTL3 with one/none (HAL1), two (HAL2), or three (HAL3) hydrogens, respectively. For the sp^2 lipid atoms, the atom type CEL1 was used with one hydrogen (HEL1). For the parametrization of ergosterol, it was necessary to introduce a new atom type (CAL1) for the atoms participating in the conjugated *cis* system of the steroid nucleus. The atom type CEL1, that normally is used to represent the sp^2 lipid atoms, is biased towards the *trans* isomer in the CHARMM27 force field. This results in the normal modes associated with the conjugated system highly deviating from the QM modes, making the introduction of a new atom type necessary. For the new atom type CAL1, LJ parameters of the sp^2 carbon atom type CEL1 were used. For all other parameters of ergosterol, existing atom types were used.

Results

Derivation of the Parameters

Parametrization of Cholesterol

Parameters for cholesterol were developed using a four-step procedure. Initially, the charges were calculated on the QM-optimized structure with the CHELPG method. The AFMM method was then used to obtain a first complete set of parameters. In the third step parameters for the hydroxyl group rotation were further refined using single-point QM energy calculations performed on hexanol. Finally, all remaining parameters were rerefined using AFMM. Atom-type assignments and partial atomic charges for cholesterol are listed in Table 1. Final (refined) values for the new parameters for cholesterol can be found in Tables 2 to 5.

The atom numbering scheme is shown in Figure 1a. The $v_j^{\max}$ vs. v_i plot for the refined cholesterol parameters is shown in Figure 2a. The corresponding value of $\sigma = 40$ cm^{-1} is lower than obtained in previous parametrization studies on molecules of similar size.[32]

Table 1. Grouping, Atom Type Assignments, and Partial Atomic Charges for Cholesterol.

Group	Atom name	Atom type	Charge	Group	Atom name	Atom type	Charge
Group 1	C_1	CTL2	−0.118	Group 2	C_2	CTL2	−0.162
	H_{C_1}	HAL2	0.059		H_{C_2}	HAL2	0.081
	H_{C_1}	HAL2	0.059		H_{C_2}	HAL2	0.081
Group 3	C_3	CTL1	−0.008	Group 4	C_5	CEL1	−0.092
	H_{C_3}	HAL1	0.180		C_6	CEL1	−0.083
	O	OHL	−0.566		H_{C_6}	HEL1	0.088
	H	HOL	0.394		C_{10}	CTL1	0.087
Group 5	C_4	CTL2	−0.200	Group 6	C_{12}	CTL2	0.036
	H_{C_4}	HAL2	0.100		$H_{C_{12}}$	HAL2	−0.018
	H_{C_4}	HAL2	0.100		$H_{C_{12}}$	HAL2	−0.018
Group 7	C_7	CTL2	−0.187	Group 8	C_9	CTL1	−0.159
	H_{C_7}	HAL2	0.092		H_{C_9}	HAL1	0.104
	H_{C_7}	HAL2	0.103		C_{11}	CTL2	0.036
	C_8	CTL1	−0.190		$H_{C_{11}}$	HAL2	0.012
	H_{C_8}	HAL1	0.183		$H_{C_{11}}$	HAL2	0.007
Group 9	C_{14}	CTL1	−0.204	Group 10	C_{15}	CTL2	−0.134
	$H_{C_{14}}$	HAL1	0.121		$H_{C_{15}}$	HAL3	0.067
	C_{13}	CTL1	0.083		$H_{C_{15}}$	HAL3	0.067
Group 11	C_{16}	CTL2	−0.108	Group 12	C_{22}	CTL2	0.042
	$H_{C_{16}}$	HAL2	0.054		$H_{C_{22}}$	HAL2	−0.021
	$H_{C_{16}}$	HAL2	0.054		$H_{C_{22}}$	HAL2	−0.021
Group 13	C_{20}	CTL1	−0.017	Group 14	C_{21}	CTL3	−0.144
	$H_{C_{20}}$	HAL1	0.029		$H_{C_{21}}$	HAL3	0.048
	C_{17}	CTL1	−0.075		$H_{C_{21}}$	HAL3	0.048
	$H_{C_{17}}$	HAL1	0.063		$H_{C_{21}}$	HAL3	0.048
Group 15	C_{18}	CTL3	−0.018	Group 16	C_{19}	CTL3	−0.144
	$H_{C_{18}}$	HAL3	0.006		$H_{C_{19}}$	HAL3	0.048
	$H_{C_{18}}$	HAL3	0.006		$H_{C_{19}}$	HAL3	0.048
	$H_{C_{18}}$	HAL3	0.006		$H_{C_{19}}$	HAL3	0.048
Group 17	C_{23}	CTL2	0.010	Group 18	C_{24}	CTL2	−0.014
	$H_{C_{23}}$	HAL2	−0.005		$H_{C_{24}}$	HAL2	0.007
	$H_{C_{23}}$	HAL2	−0.005		$H_{C_{24}}$	HAL2	0.007
Group 19	C_{26}	CTL3	0.033	Group 20	C_{27}	CTL3	0.054
	$H_{C_{26}}$	HAL3	−0.011		$H_{C_{27}}$	HAL3	−0.018
	$H_{C_{26}}$	HAL3	−0.011		$H_{C_{27}}$	HAL3	−0.018
	$H_{C_{26}}$	HAL3	−0.011		$H_{C_{27}}$	HAL3	−0.018
Group 21	C_{25}	CTL1	−0.007				
	$H_{C_{25}}$	HAL1	0.007				

Subscripts of the hydrogen atoms indicate to which carbon atoms the hydrogen atom are bonded.

Table 2. CHARMM27 Bond Parameters for Cholesterol, Ergosterol, and Lanosterol.

Bonds	K_b [kcal/mol Å^2]	b_0 [Å]
CEL1—CTL1	283.389	1.500
CAL1—CAL1	360.325	1.340
CAL1—CTL2	360.500	1.500
CAL1—CTL1	218.773	1.500
HEL1—CAL1	360.282	1.100
OHL—HOL	504.484	0.690

Only parameters not already published are listed.

Special care was taken to reproduce correctly the torsional potential of the hydroxyl group region. The rotation around this dihedral is very important because it can influence the residence time and stability of the hydrogen bonds between cholesterol and water and lipid head groups in a membrane simulation. The cholesterol hydroxyl hydrogen atom can adopt three conformations with minimum energy (i.e., *gauche*$^+$, *anti,* and *gauche*$^-$) with respect to C_2. To check the accuracy of the parameter set in this region, we calculated the rotational energy barrier of the H–O–C_3–C_2 dihedral, using both molecular mechanics and quantum chemistry. To reduce computational time, these calculations were performed using hexanol as a model of the first sterol ring.

The torsional force constants [K_χ in eq. (1)] were derived from the energy barrier for rotation of the above-mentioned dihedral at the DFT/SBJKC level of theory using single-point calculations of

Table 3. CHARMM27 Angle Parameters for Cholesterol, Ergosterol, and Lanosterol.

Angles	K_θ [kcal/mol rad^2]	θ_0 [deg]	K_{ub} [kcal/mol Å^2]	S_0 (Å)
CEL1—CEL1—CTL1	36.346	123.0		
CTL2—CEL1—CTL1	54.051	116.0		
CTL1—CTL2—CEL1	23.072	111.0		
CTL2—CTL1—CEL1	27.856	108.0		
CEL1—CTL1—CTL3	72.030	112.2		
CEL1—CTL1—CTL1	57.137	110.0		
CTL3—CTL1—CTL3	41.205	110.0	11.16	2.561
CAL1—CAL1—CAL1	67.646	121.0		
CTL1—CAL1—CTL1	42.102	118.0		
CEL1—CTL1—HAL1	53.267	107.0		
CAL1—CTL1—HAL1	29.270	107.0		
CTL1—CEL1—HEL1	23.697	120.0		
CTL1—CAL1—HEL1	20.313	120.0		
HEL1—CAL1—CAL1	33.920	119.5		
CAL1—CAL1—CTL1	73.148	123.0		
CTL2—CAL1—CTL1	54.051	116.0		
CTL1—CTL2—CAL1	23.072	111.0		
CTL2—CTL1—CAL1	56.185	108.0		
CAL1—CTL1—CTL3	22.746	112.2		
CAL1—CTL1—CTL1	73.676	110.0		
CTL3—CEL1—CTL3	33.260	111.0		
OHL—CTL1—CTL1	63.985	112.0		

the geometry-optimized structures. The remaining missing CHARMM parameters were reoptimized using AFMM. The rotational energy barrier of the H–O–C_3–C_2 dihedral after the final parametrization is shown in Figure 2b. In CHARMM, the dihedral potential energy term has the functional form: $K_\chi(1 + \cos(n\chi - \chi_0))$. To obtain an improved fit to the rotational barrier, the H–O–C_3–C_2 dihedral potential is represented as a combination of two terms (see Table 5).

Parametrization of Ergosterol

Most of the CHARMM parameters for ergosterol are the same as those for cholesterol, and thus they were directly transferred from the optimized cholesterol parameters, given the similarity of the two molecules. To derive parameters that were still missing and to save computational time, calculations were performed on the ergosterol molecule truncated to the steroid ring part, that is, 2,3,3a,4,5,5a,6,9b-octahydro-3a,6-dimethyl-1*H*-cyclopenta-[*a*]naphthalene (NP), and to the alkyl tail part (4-methyl pent-2-ene) (see Fig. 1c and d, respectively).

As mentioned in the Parameter Refinement section, the ergosterol molecule has a conjugated π system in its second steroid ring, with two *cis* hydrogens on C_6 and C_7. Initial parametrization of the ergosterol molecule, using the CHARMM atom type CEL1 for all the double bonds in the system, showed high deviation of certain normal modes from the QM reference vibrations. After visual inspection of the motions involved in the exchanged modes with the Molden program, we attributed this mismatch to vibrations located in the conjugated π system. The current implementation of the CEL1 atom type is biased towards accurate representation of the *trans* isomer. Therefore, modeling a system containing both *cis* and *trans* bonds required the introduction of a new atom type, CAL1, which corresponds to the conjugated π system. For all other atoms existing atom types were used. Due to the similarity of cholesterol and ergosterol in C_3, C_4, C_5, and C_6, the parameters optimized for these carbons for the cholesterol molecule were directly transferred to ergosterol. Atom-type assignments and partial atomic charges for ergosterol are listed in Table 6. Final (refined) values for the new parameters for ergosterol can be found in Tables 3 to 5.

Table 4. CHARMM27 Improper Torsion Parameters for Cholesterol, Ergosterol, and Lanosterol.

Improper torsions	Molecule	Atoms	K_ψ [kcal/mol rad^2]	ψ_0 [deg]
CTL3—CTL1—CTL1—CEL1	Cholesterol	C19—C9—C10—C5	2.218	−120.0
CTL3—CTL1—CTL1—CTL1	Cholesterol	C18—C17—C13—C14	7.645	−50.0
OHL—CTL2—CTL1—CTL2	Cholesterol	O—C4—C3—C2	3.000	125.0
CEL1—CTL1—CEL1—CTL2	Cholesterol	C6—C10—C5—C4	3.000	130.0
HAL1—CTL1—CTL1—CTL1	Cholesterol	H11—C9—C8—C14	3.000	−120.0
CTL2—CTL1—CTL1—CTL1	Cholesterol	C15—C13—C14—C8	3.000	130.0
CEL1—CTL2—CEL1—HEL1	Cholesterol	C5—C6—C7—HE1	20.176	180.0
CTL1—CTL2—CTL1—CTL1	Cholesterol	C20—C16—C17—C13	2.986	−130.0
CTL3—CTL2—CTL1—CTL1	Cholesterol	C21—C22—C20—C17	3.000	125.0
CTL2—CEL1—CEL1—CTL1	Cholesterol	C4—C6—C5—C10	60.599	180.0
OHL—CTL2—CTL1—CTL2	Ergosterol	O—C4—C3—C2	3.000	125.0
CTL1—CTL2—CTL1—CTL1	Ergosterol	C20—C16—C17—C13	2.986	−130.0
CAL1—CAL1—CAL1—CAL1	Ergosterol	C5—C6—C7—C8	0.500	0.0
CAL1—CAL1—CAL1—HEL1	Ergosterol	C5—C6—C7—HE1	2.345	180.0
CAL1—CAL1—CAL1—HEL1	Ergosterol	C8—C7—C6—H15	2.345	180.0
HEL1—CEL1—CEL1—HEL1	Ergosterol	H31—C22—C23—H32	5.044	180.0
OHL—CTL1—CTL1—CTL2	Lanosterol	O—C4—C3—C2	3.220	150.0
CTL3—CTL1—CTL1—CTL1	Lanosterol	C21—C22—C20—C17	3.000	125.0

Table 5. CHARMM27 Dihedral Angle Parameters for Cholesterol, Ergosterol, and Lanosterol.

Dihedral angles	K_χ [kcal/mol]	n	χ_0 [deg]	Molecule
CTL2—CTL1—CEL1—CTL2	0.500	3	0.0	
CTL3—CTL1—CEL1—CTL2	0.500	3	0.0	
CTL1—CTL2—CEL1—CTL1	0.500	3	0.0	
CTL1—CTL1—CEL1—CTL2	0.500	3	0.0	
CTL1—CTL1—CEL1—CEL1	1.000	3	0.0	
CTL2—CTL1—CEL1—CEL1	1.000	3	0.0	
CTL3—CTL1—CEL1—CEL1	0.860	3	0.0	
CTL1—CTL2—CEL1—CEL1	0.247	3	0.0	
HAL2—CTL2—CEL1—CTL1	0.294	3	0.0	
CTL2—CTL1—OHL—HOL	0.23	3	0.0	c/e
HAL1—CTL1—OHL—HOL	0.23	3	0.0	c/e
HAL1—CTL1—OHL—HOL	1.3	1	180.0	c/e
CTL2—CEL1—CEL1—HEL1	1.063	2	180.0	
CTL1—CEL1—CEL1—HEL1	0.707	2	180.0	
HEL1—CEL1—CTL2—CTL1	0.422	3	0.0	
CTL1—CTL1—CEL1—CTL1	1.003	3	0.0	
HAL1—CTL1—CEL1—CTL1	0.099	3	0.0	
CTL1—CEL1—CTL1—CTL2	1.328	3	0.0	
HAL1—CTL1—CEL1—HEL1	0.130	3	0.0	
CTL1—CTL1—CEL1—HEL1	0.015	3	0.0	
CTL3—CTL1—CEL1—HEL1	0.037	3	0.0	
CEL1—CEL1—CTL1—HAL1	0.015	3	0.0	
HEL1—CAL1—CAL1—HEL1	1.969	2	180.0	
X—CAL1—CAL1—X	7.121	2	180.0	
X—CEL1—CEL1—X	9.750	2	180.0	e
X—CEL1—CEL1—X	0.130	1	180.0	e
CAL1—CAL1—CTL2—HAL2	0.030	3	0.0	
CTL2—CTL1—CAL1—CTL2	0.500	3	0.0	
CTL3—CTL1—CAL1—CTL2	0.500	3	0.0	
CTL1—CTL2—CAL1—CTL1	0.500	3	0.0	
CTL1—CTL1—CAL1—CTL2	0.500	3	0.0	
CTL1—CTL1—CAL1—CAL1	1.129	3	0.0	
CTL2—CTL1—CAL1—CAL1	0.945	3	0.0	
CTL3—CTL1—CAL1—CAL1	0.122	3	0.0	
CTL1—CTL2—CAL1—CAL1	0.247	3	0.0	
HAL2—CTL2—CAL1—CTL1	0.294	3	0.0	
CTL1—CAL1—CAL1—HEL1	0.707	2	180.0	
CTL1—CEL1—CEL1—HEL1	0.707	2	180.0	
HEL1—CEL1—CTL2—CTL1	0.422	3	0.0	
CTL1—CTL1—CAL1—CTL1	1.033	3	0.0	
HAL1—CTL1—CAL1—CTL1	0.1667	3	0.0	
CTL1—CAL1—CTL1—CTL2	1.4857	3	0.0	
HAL1—CTL1—CAL1—HEL1	0.130	3	0.0	
CTL3—CTL1—CAL1—HEL1	0.037	3	0.0	
CAL1—CAL1—CTL1—HAL1	0.015	3	0.0	
HOL—OHL—CTL1—CTL1	0.16	3	0.0	l
HOL—OHL—CTL1—CTL2	0.24	3	0.0	l
HAL1—CTL1—OHL—HOL	0.24	3	0.0	l
HAL1—CTL1—OHL—HOL	0.5	1	120.0	l
HAL1—CTL1—OHL—HOL	0.7	1	220.0	l
HAL1—CTL1—OHL—HOL	0.12	2	0.0	l
HAL1—CTL1—OHL—HOL	0.15	2	90.0	l
CTL2—CTL2—CEL1—CTL1	1.815	3	0.0	
HAL3—CTL3—CEL1—CTL3	0.155	3	0.0	
CTL2—CEL1—CTL1—HAL1	3.233	3	0.0	

The last column indicates parameters that are common for the three molecules but may used only for the indicated molecule: cholesterol (c), ergosterol (e), and lanosterol (l).

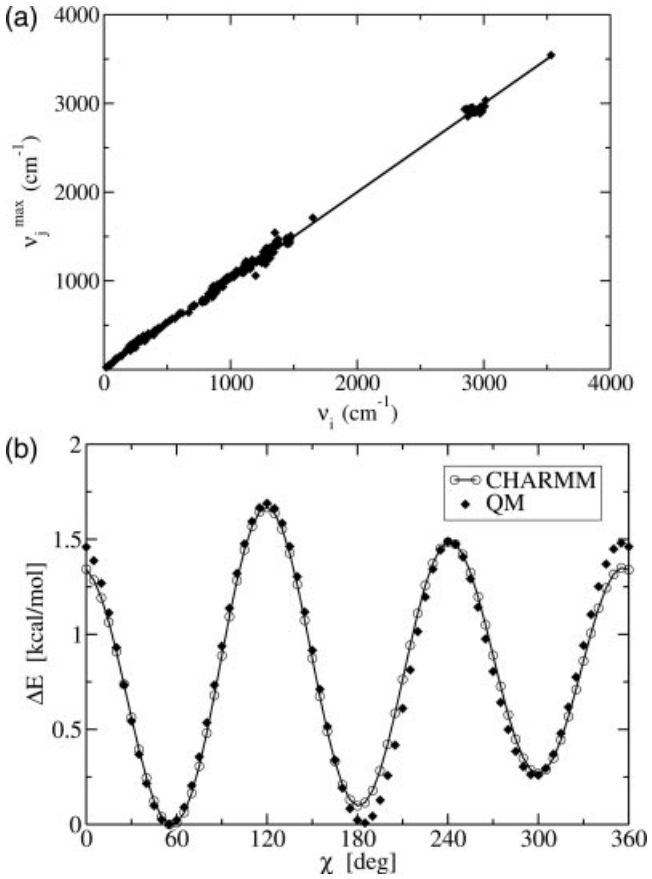

Figure 2. (a) Frequency matching plot (v_j^{max} vs. v_i) for cholesterol. The line is the ideal case of perfectly matched frequencies and eigenvector projections. Points refer to the optimized parameter set. σ = 40.0 cm^{-1}, (b) rotational energy barrier along the C_2—C_3—O—H dihedral angle for cyclohexanol. The filled diamonds are the QM points calculated with NWChem. The open circles and the line are the fitted CHARMM potential.

The resulting v_j^{max} vs. v_i plots after the parameter optimization of NP and of 4-methyl pent-2-ene are shown in Figure 3a and b, respectively. The corresponding values of σ = 38.7 cm^{-1} and of σ = 58.5 cm^{-1} are within the σ-values obtained in previous parametrization studies of similarly sized molecules.[32]

Parametrization of Lanosterol

For the parametrization of lanosterol, parameters developed for both cholesterol and ergosterol were transferred and only parameters not existing previously were optimized. For computational efficiency lanosterol was parametrized using two smaller molecules: 2,2 dimethyl cyclohexanol and 2 methyl 3 isopropyl hex-2-ene (Fig. 1f and g, respectively). The resulting v_j^{max} vs. v_i plots for the two molecules are shown in Figure 4a (σ = 41.2 cm^{-1}) and b (σ = 61.2 cm^{-1}), respectively.

The first steroid ring of lanosterol is bulkier than that of cholesterol, containing two extra methyl groups on C_4. As in the case of cholesterol, we calculated the rotational energy barrier of the HO–O–C_3–C_2 dihedral, using both molecular mechanics and quantum chemistry. To reduce computational time, this calculation was performed using 2,2 dimethyl hexanol to model the first sterol ring. The torsional force constants [K_χ in eq. (1)] were derived from the energy barrier for rotation of the above-mentioned dihedral at the DFT/SBJKC level of theory using single-point calculations to scan the potential energy profile.

In the case of lanosterol, two twofold and two onefold dihedral terms were added to the already existing threefold term of the potential to obtain a better fit for the barrier (see Table 5). The rotational energy barrier of the H–O–C_3–C_2 dihedral after the final parametrization can be seen in Figure 4c. The 2 kcal/mol barrier arises from the unfavorable interaction between the two methyl groups on C_4 and with the hydroxyl hydrogen. The parameters adjusted to reproduce this rotational barrier were subsequently fixed and the remaining parameters optimized in CHARMM using AFMM. Atom-type assignments and partial atomic charges for lanosterol are listed in Table 7. Final (refined) values for the new parameters for lanosterol can be found in Tables 3 to 5.

Testing of the Parameters

Cholesterol Crystal Simulation

Final testing of a parameter set should be performed against independent experimental and/or theoretical data. Here, the refined potential was tested by performing an energy minimization and MD simulation of cholesterol in its crystalline state and comparing the results with the X-ray experimental results.[27] The experimental unit cell contains eight cholesterol molecules (A–H), and is triclinic with no symmetry (space group P_1) as seen in Figure 5a. In all structures of cholesterol and its solvates, the molecules adopt a bilayer arrangement generally similar to that of cholesterol in biological membranes with alternating hydrophilic and hydrophobic layers. In the hydrophilic layer of the triclinic unit cell there are four hydrogen-bonded chains parallel to the *c*-axis, with all eight hydrogen atoms of each hydroxyl group pointing towards the positive *c* direction. The molecules are hydrogen bonded in two separate chains: . . . -BHAG-BHAG- . . . and . . . -DFCE-DFCE- . . . (see Fig. 5b).

Another interesting feature of the cholesterol crystal is the presence of local pseudosymmetry, that is, noncrystallographic symmetry.[44] Each molecule in one chain is related to a molecule in the other chain by a series of parallel axes of local twofold symmetry. Thus, molecule A is related to molecule E, H to D, B to F and G to C. The pseudosymmetry operation, which applies to complete molecules, involves a rotation of 180° and a translation of about 2.8 Å parallel to the *c*-axis. This operation brings molecules A, B, C, and D into close superposition with molecules E, F, G, and H. This complex packing arrangement allows an infinite hydrogen-bonded network to be formed, with an average O . . . O distance of 2.9 Å. In the monohydrate structure of cholesterol[45] the cholesterol molecules exhibit a more regular packing due to the presence of the water molecules, which assist the hydrogen-bonded bridges.

The MD calculations were performed for the whole crystal using periodic boundary conditions. The unit cell dimensions were allowed to vary both during the energy minimization and the MD simulation. Hydrogens were constructed using idealized geometric parameters form the HBUILD module in CHARMM.

Table 6. Grouping, Atom Type Assignments, and Partial Atomic Charges for Ergosterol.

Group	Atom name	Atom type	Charge	Group	Atom name	Atom type	Charge
Group 1	C_1	CTL2	−0.056	Group 2	C_2	CTL2	−0.174
	H_{C_1}	HAL2	0.028		H_{C_2}	HAL2	0.087
	H_{C_1}	HAL2	0.028		H_{C_2}	HAL2	0.087
Group 3	C_3	CTL1	0.133	Group 4	C_5	CAL1	−0.101
	H_{C_3}	HAL1	0.055		C_6	CAL1	−0.150
	O	OHL	−0.557		H_{C_6}	HEL1	0.092
	H	HOL	0.369		C_{10}	CTL1	0.159
Group 5	C_4	CTL2	−0.174	Group 6	C_{12}	CTL2	−0.022
	H_{C_4}	HAL2	0.087		$H_{C_{12}}$	HAL2	0.011
	H_{C_4}	HAL2	0.087		$H_{C_{12}}$	HAL2	0.011
Group 7	C_7	CAL1	−0.036	Group 8	C_{16}	CTL2	−0.142
	H_{C_7}	HEL1	0.078		$H_{C_{16}}$	HAL2	0.071
	C_8	CAL1	−0.042		$H_{C_{16}}$	HAL2	0.071
Group 9	C_{14}	CTL1	−0.264	Group 10	C_{15}	CTL2	−0.186
	$H_{C_{14}}$	HAL1	0.147		$H_{C_{15}}$	HAL3	0.093
	C_{13}	CTL1	0.117		$H_{C_{15}}$	HAL3	0.093
Group 11	C_{20}	CTL1	−0.182	Group 12	C_{22}	CEL1	−0.113
	$H_{C_{20}}$	HAL1	0.131		$H_{C_{22}}$	HEL1	0.103
	C_{17}	CTL1	−0.034		C_{23}	CEL1	−0.091
	$H_{C_{17}}$	HAL1	0.085		$H_{C_{23}}$	HEL1	0.101
Group 13	C_{11}	CTL1	−0.072	Group 14	C_9	HAL2	−0.066
	$H_{C_{11}}$	HAL1	0.036		H_{C_9}	HAL2	0.066
	$H_{C_{11}}$	CTL2	0.036				
Group 15	C_{18}	CTL3	−0.174	Group 16	C_{19}	CTL3	−0.111
	$H_{C_{18}}$	HAL3	0.058		$H_{C_{19}}$	HAL3	0.037
	$H_{C_{18}}$	HAL3	0.058		$H_{C_{19}}$	HAL3	0.037
	$H_{C_{18}}$	HAL3	0.058		$H_{C_{19}}$	HAL3	0.037
Group 17	C_{25}	CTL1	−0.067	Group 18	C_{24}	CTL1	−0.067
	$H_{C_{25}}$	HAL1	0.067		$H_{C_{24}}$	HAL1	0.067
Group 19	C_{26}	CTL3	−0.069	Group 20	C_{27}	CTL3	−0.135
	$H_{C_{26}}$	HAL3	−0.023		$H_{C_{27}}$	HAL3	0.045
	$H_{C_{26}}$	HAL3	−0.023		$H_{C_{27}}$	HAL3	0.045
	$H_{C_{26}}$	HAL3	−0.023		$H_{C_{27}}$	HAL3	0.045
Group 21	C_{28}	CTL3	−0.069	Group 22	C_{21}	CTL3	−0.252
	$H_{C_{28}}$	HAL3	0.023		$H_{C_{21}}$	HAL3	0.084
	$H_{C_{28}}$	HAL3	0.023		$H_{C_{21}}$	HAL3	0.084
	$H_{C_{28}}$	HAL3	0.023		$H_{C_{21}}$	HAL3	0.084

Subscripts of the hydrogen atoms indicate to which carbon atoms the hydrogen atom are bonded.

The energy-minimized cell vectors are reported in Table 8, along with the experimental values. After minimization the cell volume was computed to be 5056.8 Å^3, within 0.5% of the experimental volume of 5032.8 Å^3. The calculated cell vectors and the volume obtained during the MD simulation are shown in Table 8. The MD simulation reproduces the hydrogen-bonded network in the cholesterol crystal. The hydrogen-bond distances are shown in Table 9. The MD H-bonds are slightly longer (0.1 Å on average) than those reported experimentally. However, we observed that the H-bonding pattern remains stable throughout the simulation. [Time-series of the O . . . O distances between the hydrogen-bonded pairs D–F, F–C, C–E from the first chain, and B–H, H–A, A–G from the second chain can be seen in Figure 1 of the supplementary material (SM)]. The average H-bonding distance is 2.9 Å for the six hydrogen bonds formed. The experimental ordering of the hydrogen-bonded distances within each of the two hydrogen-bonded chains is also preserved for example, $d_{DF} > d_{FC} > d_{CE}$. The angle between the donor hydroxyl group and the acceptor oxygen atom was found to be, on average, 160.3° for the six hydrogen bonds formed in the primary unit cell, which is close to linearity (see Table 10). Figure 2 (SM) shows the time series of these angles. Further evidence that the hydrogen bonds remain stable during the simulation comes from the observation that the dihedral C_1–C_2–C_3–O remains almost constant for all eight molecules, with a value of 175.1 ± 3.7° (see Table 11).

Hydrogen bonds link the molecules into chains along the *c*-axis and all eight hydrogen atoms of each hydroxyl group point towards the positive *c* direction. The mean value of the angle between the *a* axis of the unit cell and the O–H vector (Table 12) is 91.1°, indicating that the preferred position of the hydrogens is indeed aligned with the *c*-axis of the unit cell.

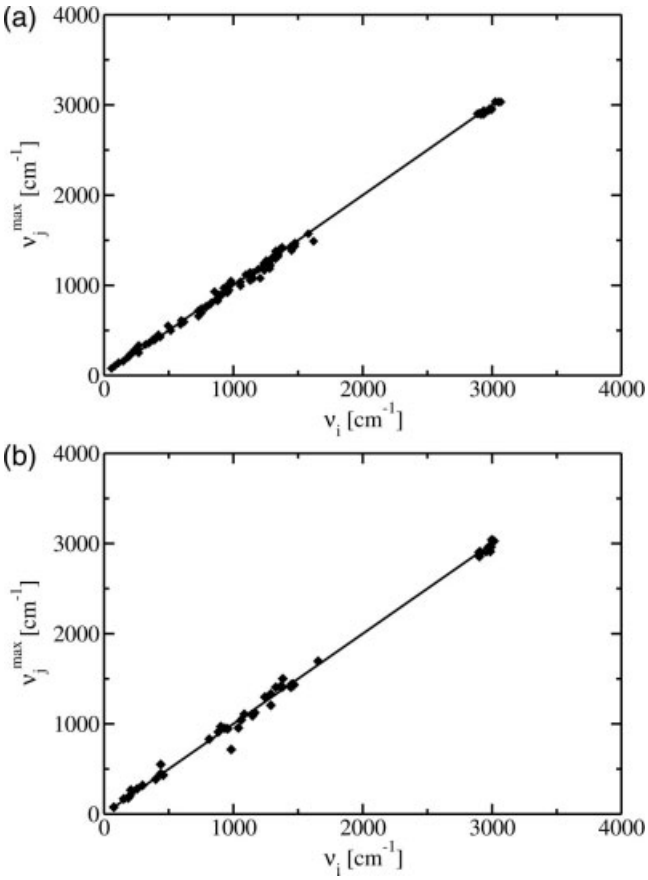

Figure 3. Frequency matching plot (v_j^{max} vs. v_i) for (a) NP (σ = 38.7 cm^{-1}) and for (b) 4-methyl pent-2-ene (σ = 58.5 cm^{-1}). The line is the ideal case of perfectly matched frequencies and eigenvector projections. Points refer to the optimized parameter set.

The distribution of the interaction energies between two hydrogen-bonded hydroxyl groups is plotted in Figure 6 for the hydrogen bonded pairs H–A, A–G, B–H from the first chain and E–C, C–F, F–D from the second. The mean value of the hydrogen-bond strength, −4.2 kcal/mol, is well within the typical hydrogen bond range (−1 to −5 kcal/mol, depending on donor and acceptor atom as well as their environment).

To examine the rigidity of the steroid rings the average values and standard deviations of the torsional angles of the steroid ring system were calculated. The low values of the deviations show that the eight steroid units are similar and do not undergo major variability. The results, shown in Table 13, are in good agreement with those obtained in the crystal structure study.[27] The hydrocarbon tail of cholesterol is expected to be flexible at room temperature and to undergo several conformational transitions. Table 14 shows the percentage of the *trans* conformation for the alkyl tail dihedrals of cholesterol. It is clear that, compared to the simulation of a single molecule in vacuum (see below), the crystal environment inhibits the *trans* to *gauche* transitions of the individual molecules due to steric hindrance arising from the packing in the crystal. The adjacent crystal molecules "lock" the conformation, for example, the pseudosymmetrically related molecules C and G adopt a *gauche*$^-$ − *trans* − *gauche*$^-$ conformation in the crystal and do not change it throughout the simulation.

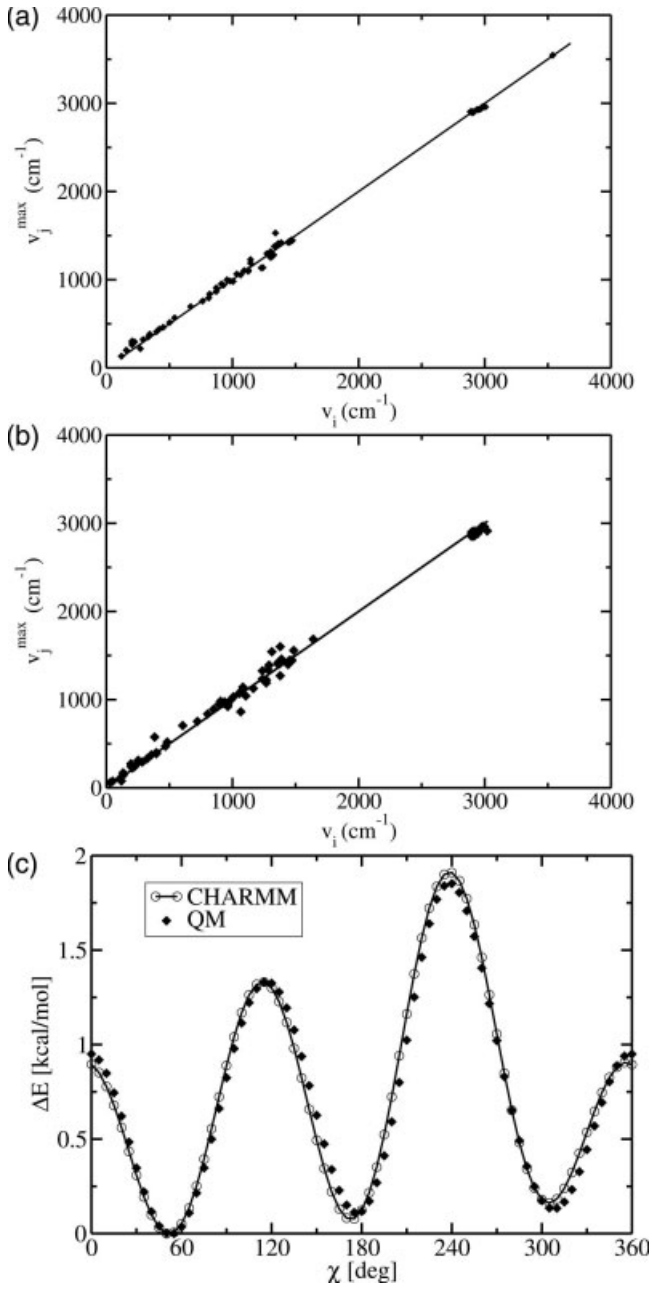

Figure 4. Frequency matching plot (v_j^{max} vs. v_i) for (a) 2,2 dimethyl hexanol (σ = 41.2 cm^{-1}) and for (b) 3-isopropyl-2-methylhex-2-ene (σ = 61.2 cm^{-1}). The line is the ideal case of perfectly matched frequencies and eigenvector projections. Points refer to the optimized parameter set. (c) Rotational energy barrier along the C_2—C_3—O—H dihedral angle of 2,2 dimethyl cyclohexanol. The filled diamonds are the quantum chemically calculated energies. The open circles and the line are the fitted CHARMM potential.

Table 7. Grouping, Atom Type Assignments, and Partial Atomic Charges for Lanosterol.

Group	Atom name	Atom type	Charge	Group	Atom name	Atom type	Charge
Group 1	C_1	CTL2	−0.148	Group 2	C_2	CTL2	−0.118
	H_{C_1}	HAL2	0.074		H_{C_2}	HAL2	0.059
	H_{C_1}	HAL2	0.074		H_{C_2}	HAL2	0.059
Group 3	C_3	CTL1	0.053	Group 4	C_4	CTL1	0.036
	H_{C_3}	HAL1	0.114		C_5	CTL1	−0.149
	O	OHL	−0.535		H_{C_5}	HAL1	0.113
	H	HOL	0.368				
Group 5	C_6	CTL2	−0.192	Group 6	C_7	CTL2	−0.082
	H_{C_6}	HAL2	0.096		H_{C_7}	HAL2	0.041
	H_{C_6}	HAL2	0.096		H_{C_7}	HAL2	0.041
Group 7	C_8	CEL1	0.096	Group 8	C_{11}	CTL3	−0.186
	C_9	CEL1	−0.082		$H_{C_{11}}$	HAL3	0.093
	C_{10}	CTL1	−0.014		$H_{C_{11}}$	HAL3	0.093
Group 9	C_{12}	CTL2	−0.096	Group 10	C_{13}	CTL1	0.018
	$H_{C_{12}}$	HAL2	0.048		C_{14}	CTL1	−0.018
	$H_{C_{12}}$	HAL2	0.048				
Group 11	C_{15}	CTL2	−0.110	Group 12	C_{16}	CTL2	−0.096
	$H_{C_{15}}$	HAL3	0.055		$H_{C_{16}}$	HAL2	0.048
	$H_{C_{15}}$	HAL3	0.055		$H_{C_{16}}$	HAL2	0.048
Group 13	C_{20}	CTL1	−0.154	Group 14	C_{21}	CTL3	−0.219
	$H_{C_{20}}$	HAL1	0.128		$H_{C_{21}}$	HAL3	0.073
	C_{17}	CTL1	−0.077		$H_{C_{21}}$	HAL3	0.073
	$H_{C_{17}}$	HAL1	0.103		$H_{C_{21}}$	HAL3	0.073
Group 15	C_{18}	CTL3	−0.165	Group 16	C_{19}	CTL3	−0.252
	$H_{C_{18}}$	HAL3	0.055		$H_{C_{19}}$	HAL3	0.084
	$H_{C_{18}}$	HAL3	0.055		$H_{C_{19}}$	HAL3	0.084
	$H_{C_{18}}$	HAL3	0.055		$H_{C_{19}}$	HAL3	0.084
Group 17	C_{22}	CTL2	−0.144	Group 18	C_{23}	CTL2	−0.102
	$H_{C_{22}}$	HAL2	0.072		$H_{C_{23}}$	HAL2	0.051
	$H_{C_{22}}$	HAL2	0.072		$H_{C_{23}}$	HAL2	0.051
Group 19	C_{24}	CEL1	−0.038	Group 20	C_{26}	CTL3	−0.309
	C_{25}	CEL1	−0.009		$H_{C_{26}}$	HAL3	0.103
	$H_{C_{25}}$	HEL1	0.047		$H_{C_{26}}$	HAL3	0.103
					$H_{C_{26}}$	HAL3	0.103
Group 21	C_{27}	CTL3	−0.195	Group 22	C_{28}	CTL3	−0.309
	$H_{C_{27}}$	HAL3	0.065		$H_{C_{28}}$	HAL3	0.103
	$H_{C_{27}}$	HAL3	0.065		$H_{C_{28}}$	HAL3	0.103
	$H_{C_{27}}$	HAL3	0.065		$H_{C_{28}}$	HAL3	0.103
Group 23	C_{29}	CTL3	−0.195	Group 24	C_{30}	CTL3	−0.123
	$H_{C_{29}}$	HAL3	0.065		$H_{C_{30}}$	HAL3	0.041
	$H_{C_{29}}$	HAL3	0.065		$H_{C_{30}}$	HAL3	0.041
	$H_{C_{29}}$	HAL3	0.065		$H_{C_{30}}$	HAL3	0.041

Subscripts of the hydrogen atoms indicate to which carbon atoms the hydrogen atom are bonded.

The atoms of the hydrocarbon tail of cholesterol are more flexible than the steroid-ring atoms. Therefore, they are expected to exhibit more freedom of movement, corresponding to spreading of the probability distribution of each atom over a small region of space. Diffraction is affected by this spreading out of the atomic positions, as manifested by temperature factors (B-factors), assigned to each atom. Assuming isotropic, harmonic dynamics, the B-factor is given by:

$$B_{eq} = \frac{8\pi^2}{3}\langle u^2 \rangle \tag{4}$$

where $\langle u^2 \rangle$ is the mean-square fluctuation of the position of an atom.

In Figure 7a, the average experimental and calculated isotropic B-factors for the oxygen and the carbon atoms of cholesterol are shown. Figure 7b shows the unit cell colored by B-factor: red indicates high values of B_{eq} and blue low values of B_{eq}. Both representations indicate parts of the molecule that are particularly flexible and parts that are particularly rigid. The side-chain B-factors are larger and more varied (10 to 45 Å^2) than those of the rigid steroid ring atoms (3 to 9 Å^2). The B-factors obtained from MD are somewhat larger than those derived experimentally for the

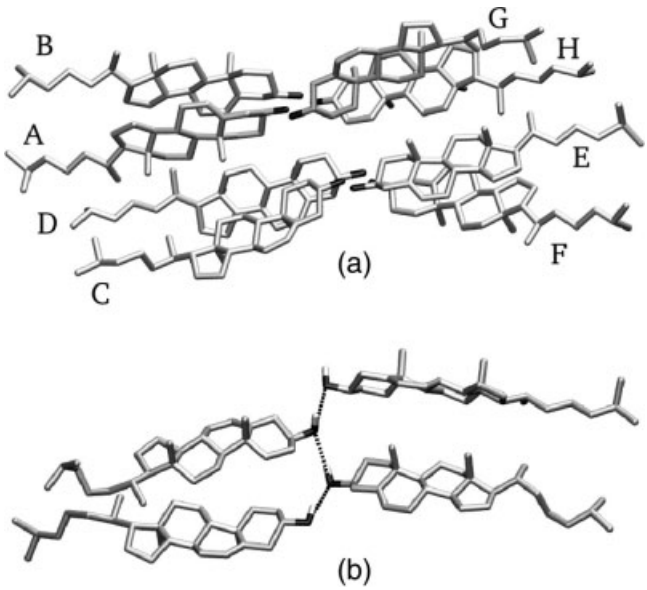

Figure 5. (a) Experimental unit cell of the crystal structure of cholesterol projected on the *a*, *b* plane. The crystal structure is that of ref. 27. The letters A, B, C, D, E, F, G, and H mark the crystallographically resolved molecules. (b) Hydrogen bonding scheme for molecules D, F, C, and E (top to bottom) in the crystal structure of cholesterol.

ends of the flexible tails. These differences may arise from the use of isotropic, harmonic approximation in the experimental refinement; this approximation is invalid for barrier-crossing dynamics (e.g., *trans–gauche* dynamics).

The root-mean-square deviation (RMSD):

$$\mathrm{RMSD} = \sqrt{\frac{1}{N}\sum_{i=1}^{N}(x_i - \bar{x})^2} \qquad (5)$$

between the experimental and calculated average structure and experimental nonhydrogen atom positions in the unit cell was found to be 0.45 Å, but after comparison only to atoms with experimental $B_{eq} < 10$ Å^2 the RMSD becomes 0.22 Å. After removing the rotation and translation of the individual molecules in the unit cell, the RMSD was 0.33 Å including all heavy atoms and 0.13 Å when including only atoms with $B_{eq} < 15$ Å^2. Averaging the coordinates of the eight cholesterol molecules over all the trajectory, and calculating the RMSD with respect to the average experimental coordinates of one cholesterol molecule, including all nonhydrogen atoms with $B_{eq} < 15$ Å, the RMSD reduces significantly, to 0.07 Å.

Molecular crystals are held together due to attractive nonbonded energies between the molecules (electrostatic, van der Waals forces). Because the cholesterol crystal has a high melting point (around 140°C), these energies must be relatively strong. The average interaction energy between a cholesterol molecule and the rest of the crystal was found to be -53.7 ± 0.6 kcal/mol, from which 85% arises from van der Waals interactions and 15% from electrostatics.

To further examine the nature of the nonbonded interactions in the cholesterol crystal, interaction energies between the different cholesterol molecules were calculated. Adjacent molecules along the positive *c*-axis (i.e., on top of each other) form four chains: . . . ABAB . . . (I), . . . CDCD . . . (II), . . . EFEF . . . (III), and . . . HGHG . . . (IV), and each cholesterol pair in these chains has negative van der Waals energies. In chains I and III, the cholesterol molecules interact as seen in Figure 8d and in chains II and IV as seen in Figure 8b. The molecules in these two groups of chains contain molecules that are pseudosymmetrically related between them. The time series of the interaction energy between molecules A and B, E, and F (of chains I and III) and between molecules C

Table 8. Cell Vectors for the Cholesterol X-ray Diffraction at Room Temperature and After Energy Minimization and MD Using the New CHARMM Force Field.

Cell dimension	Experimental values	Energy minimization	Molecular dynamics
a	14.172 Å	13.94 Å	(14.26 ± 0.21) Å
b	34.209 Å	35.03 Å	(34.24 ± 0.49) Å
c	10.481 Å	10.39 Å	(10.73 ± 0.14) Å
α	94.64°	93.70°	(94.61 ± 1.83)°
β	90.67°	91.46°	(90.99 ± 1.63)°
γ	96.32°	91.38°	(97.03 ± 1.85)°

Table 9. O · · · O Distances between Hydrogen Bonded Pairs in Angstroms.

H-bond pair	X-ray	Molecular dynamics
A—G	2.97	3.01 ± 0.18
B—H	2.82	2.93 ± 0.16
C—E	2.76	2.91 ± 0.15
D—F	2.90	2.97 ± 0.17
F—C	2.88	2.93 ± 0.16
H—A	2.79	2.88 ± 0.14

Experimental values, values after energy minimization, and mean values and standard deviations from the molecular dynamics simulation.

Table 10. O-H . . . O Angles between Hydrogen Bonded Pairs in Degrees.

H-bond pair	Molecular dynamics
A—G	163.8 ± 9.1
B—H	156.4 ± 10.8
C—E	164.7 ± 8.3
D—F	151.8 ± 11.3
F—C	160.8 ± 9.3
H—A	164.4 ± 8.5

Mean values and standard deviations from the molecular dynamics simulation.

Table 11. C_1—C_2—C_3—O Dihedral Angle Value in Degrees.

Molecule	Experimental	Minimization	Molecular dynamics
D	179.4	179.6	175.7 ± 3.3
F	177.5	177.8	175.5 ± 3.4
C	178.7	176.1	174.8 ± 3.9
E	179.8	177.6	174.7 ± 3.9
H	176.5	179.0	175.5 ± 3.4
B	179.3	177.8	175.5 ± 3.4
G	177.2	176.6	174.9 ± 3.8
A	179.9	178.0	174.7 ± 3.9

Experimental values, mean values, and standard deviations from the molecular dynamics simulation.

and D, H and G (of chains II and IV) in the primary unit cell are shown in Figure 8c and a, respectively. The interaction energy is averaged over the two pseudosymmetrically-related pairs. Adjacent image molecules that contribute to the interaction energy are included in the calculation. Further decomposition of the interaction energy of these pairs into the van der Waals and electrostatic contributions shows that the electrostatic interaction energy is small, and the main stabilizing energetic contribution arises from the van der Waals energy. In addition, the main van der Waals contribution to the interaction energy was found to arise from the ring–ring interaction between molecules that are on top of each other. The van der Waals interaction energies between two adjacent molecules in chains I and III and chains II and IV have mean values of −10 kcal/mol and −8.5 kcal/mol, respectively. This interaction energy is more than double the mean hydrogen-bond energy between cholesterol molecules in the crystal.

The interaction energy between molecules that are hydrogen bonded along the *c*-axis is mainly electrostatic. The average interaction energy of all eight hydrogen-bonded pairs is −4.1 ± 0.1 kcal/mol. The electrostatic contribution to the average interaction energy of all hydrogen-bonded pairs is −4.9 ± 0.3 kcal/mol, while the van der Waals contribution accounts for 0.8 ± 0.2 kcal/mol. As an example, the distribution of the total interaction energy of the hydrogen bonded pair B and H along with the electrostatic and van

Table 12. Angles between Hydrogen Atoms of the Hydroxyl Group with Respect to the *a*-Axis, in Degrees.

Molecule	θ
A	88.0 ± 10.9
B	111.0 ± 16.9
C	102.3 ± 11.0
D	89.1 ± 13.4
E	86.7 ± 10.4
F	83.8 ± 20.0
G	80.4 ± 10.5
H	87.5 ± 13.3

Mean values and standard deviations from the molecular dynamics simulation.

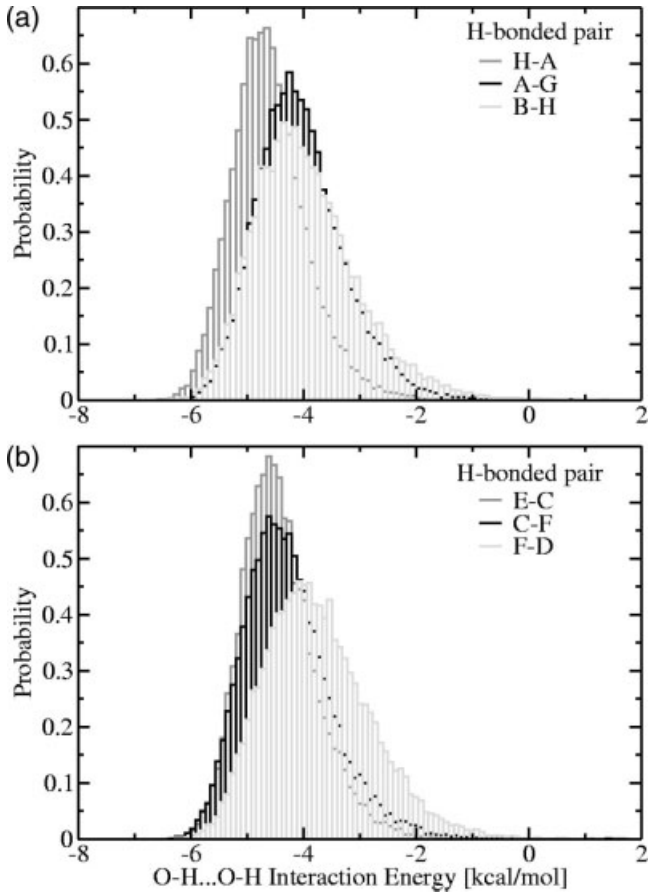

Figure 6. Probabilities of interaction energies for the hydrogen-bonded hydroxyl pairs in the primary unit cell (a) between molecules H—A (−4.6 ± 0.7 kcal/mol), A—G (−4.1 ± 0.8 kcal/mol), B—H (−4.0 ± 0.9 kcal/mol), and (b) in the second chain between molecules E—C (−4.4 ± 0.7 kcal/mol), C—F (−4.3 ± 0.8 kcal/mol), F—D (−3.7 ± 0.9 kcal/mol). The values in the parentheses correspond to mean values and standard deviations.

der Waals contributions can be seen in Figure 3 of the Supplementary Material. Along the *c*-axis the favorable forces in the cholesterol crystal are the hydrogen-bonded network and the van der Waals interactions between the rings of adjacent molecules. Figure 9a shows three unit cells projected on the (*c*, *b*) plane. Hydrogens have been omitted from the representation for clarity.

Along the *a* axis in the primary unit cell, molecules B and D, F and H, C and A, E and G are adjacent (see Fig. 5a). The interaction energy between adjacent, along the *a*-axis, cholesterol molecules arises mainly from van der Waals contributions. For example, the van der Waals interaction energy between adjacent molecules B and D is, on average, −4.2 ± 0.6 kcal/mol, and the electrostatic interaction energy 0.4 ± 0.1 kcal/mol (see Fig. 4 of SM). When constructing the crystal lattice, the corresponding transformations following the geometry of the unit cell place the ring of molecule C next to the hydrogen-bonded molecules A and G of the next unit cell, as well as placing the ring of molecule A next to the hydrogen bond between molecules C and E of the

Table 13. Torsional Angles (in degrees) in the Rings of the Steroid Ring System, Averaged over the Eight Molecules.

Torsion angle	Experiment	MD of crystal	MD of single molecule
C_1—C_2—C_3—C_4	58 ± 2	55.9 ± 5.2	56.6 ± 5.7
C_2—C_3—C_4—C_5	−56 ± 2	−54.7 ± 5.6	−54.6 ± 6.3
C_3—C_4—C_5—C_{10}	53 ± 1	53.0 ± 5.3	51.0 ± 6.3
C_4—C_5—C_{10}—C_1	−48 ± 3	−47.6 ± 4.6	−45.5 ± 5.6
C_5—C_{10}—C_1—C_2	49 ± 4	48.7 ± 5.4	47.8 ± 6.2
C_5—C_6—C_7—C_8	13 ± 1	15.7 ± 5.3	12.6 ± 6.5
C_6—C_7—C_8—C_9	−43 ± 2	−44.0 ± 5.5	−39.9 ± 7.0
C_7—C_8—C_9—C_{10}	62 ± 1	60.8 ± 4.5	58.9 ± 5.0
C_8—C_9—C_{10}—C_5	−47 ± 2	−45.8 ± 4.9	−47.4 ± 5.7
C_8—C_{14}—C_{13}—C_{12}	−61 ± 1	−59.4 ± 4.3	−59.5 ± 4.4
C_9—C_8—C_{14}—C_{13}	57 ± 1	55.2 ± 4.7	56.1 ± 4.8
C_9—C_{10}—C_5—C_6	16 ± 2	16.7 ± 4.8	19.4 ± 5.9
C_{10}—C_1—C_2—C_3	−56 ± 2	−55.3 ± 5.7	−55.6 ± 6.1
C_{10}—C_5—C_6—C_7	1 ± 2	−1.9 ± 3.5	−2.2 ± 3.7
C_{11}—C_9—C_8—C_{14}	−49 ± 1	−46.5 ± 5.0	−48.1 ± 5.3
C_{12}—C_{11}—C_9—C_8	50 ± 2	47.1 ± 6.0	48.4 ± 6.1
C_{13}—C_{12}—C_{11}—C_9	−55 ± 1	−51.3 ± 5.7	−51.5 ± 5.7
C_{13}—C_{14}—C_{15}—C_{13}	−34 ± 1	−30.3 ± 5.7	−30.5 ± 5.9
C_{14}—C_{13}—C_{12}—C_{11}	56 ± 1	54.9 ± 4.6	54.4 ± 4.8
C_{14}—C_{15}—C_{16}—C_{17}	8 ± 2	5.2 ± 6.8	5.9 ± 7.1
C_{15}—C_{16}—C_{17}—C_{13}	21 ± 2	20.8 ± 6.5	20.0 ± 7.0
C_{16}—C_{17}—C_{13}—C_{14}	−41 ± 2	−37.5 ± 4.3	−37.0 ± 4.8
C_{17}—C_{13}—C_{14}—C_{15}	47 ± 1	42.3 ± 3.8	42.1 ± 4.0

Experimental values and mean values from the molecular dynamics simulations of crystal and of single molecule.

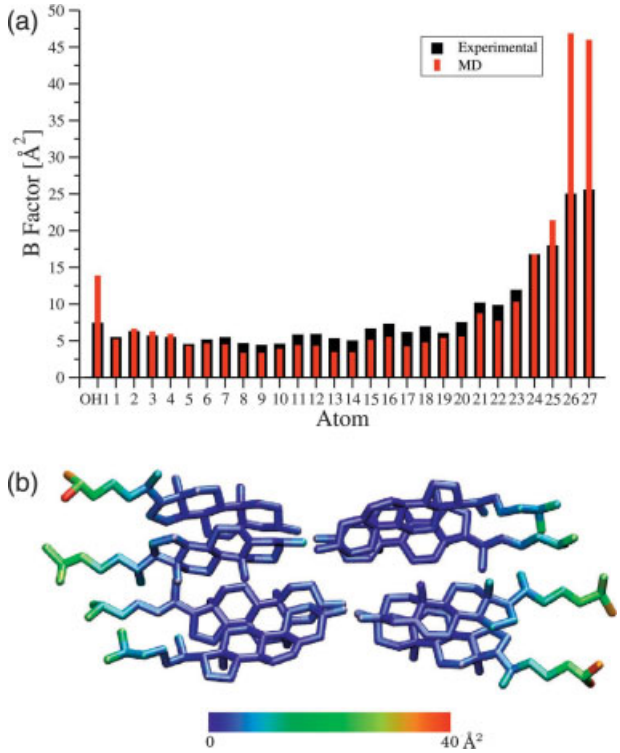

Figure 7. (a) Experimental vs. the calculated average B-factors for the oxygen and the carbon atoms. (b) The experimental unit cell colored according to the experimentally determined B-factors (Å^2). Red ("hot") corresponds to high values of B-factors, and blue ("cold") corresponds to low values of B-factor. The color scale is given at the bottom.

neighboring unit cell (see Fig. 9b). The interaction energy between these pairs was also calculated, and it was found that, again, the van der Waals interactions dominate. The van der Waals interaction energy between molecule C of the primary unit cell and molecule G of the image unit cell was found to be on average −5.0 ± 0.6 kcal/mol and the electrostatic interaction energy just 0.3 ± 0.1 kcal/mol (see Fig. 5 of SM). It is interesting to note that, in both cases, the van der Waals contribution to the interaction energy has the approximate strength of a hydrogen bond.

Along the *b*-axis (i.e., the long axis of the unit cell) the crystal forms an alternating network of hydrophobic and hydrophilic layers (Fig. 9c). The hydrocarbon chains are staggered, resulting to significant interdigitation in the hydrophobic layer. Specifically, the tails of the molecules B and F from the primary unit cell come in to close contact with the tails of the image molecules F and B, respectively (see Fig. 10c). The tail of molecule F comes near the tail of molecule A, the one of molecule H to molecule A, molecule D to E, A to E, B to G and B to E. The interaction energy between the tails of the molecules is also found to be favorable and to arise mainly from van der Waals forces.

The above observations allow us to conclude that the dominating energy contribution to the total interaction energy in the cholesterol crystal is the negative van der Waals interaction between neighboring molecules. Electrostatics contribute ≈15% to the total interaction energy, arising from the hydrogen-bonded network.

Table 14. Percentages (%) of *trans* Conformations for the Alkyl Tail of Cholesterol.

Carbon atoms	Single molecule	A	B	C	D	E	F	G	H
C_{17}—C_{20}—C_{22}—C_{23}	96.2	100.0	100.0	0.0	100.0	100.0	100.0	0.0	100.0
C_{20}—C_{22}—C_{23}—C_{24}	68.0	84.4	99.6	100.0	92.0	83.6	100.0	100.0	100.0
C_{22}—C_{23}—C_{24}—C_{25}	84.6	93.5	92.8	0.0	96.4	98.5	22.1	0.0	100.0
C_{23}—C_{24}—C_{25}—C_{26}	33.0	51.9	59.5	0.0	16.7	21.8	13.2	0.0	1.0

The A—H columns refer to the molecules from the molecular dynamics simulation of the crystal.

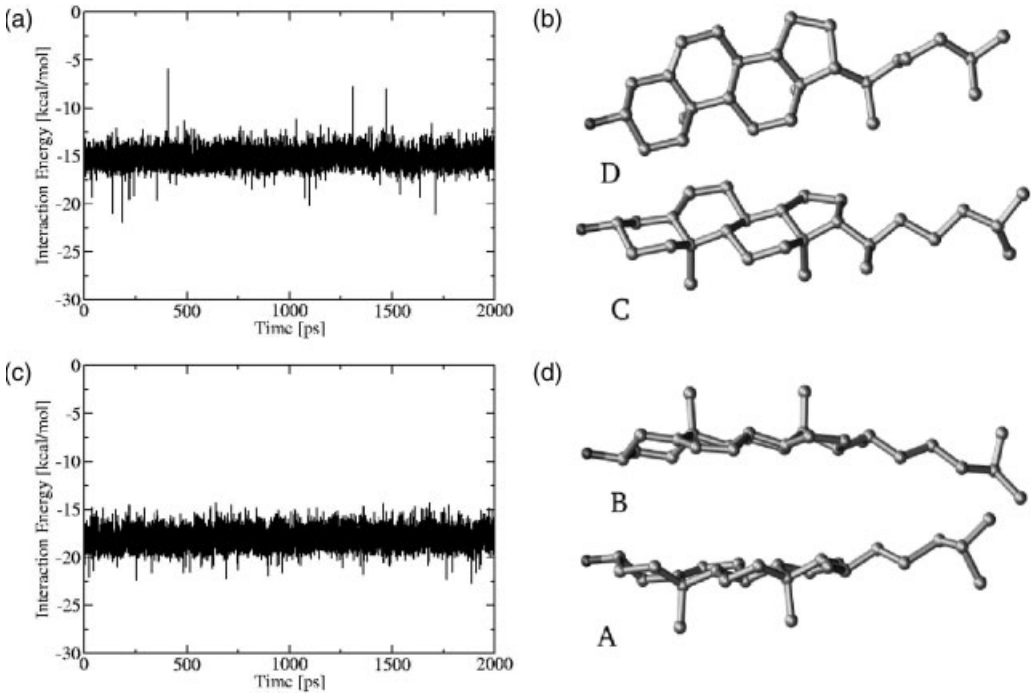

Figure 8. (a) Time series of the interaction energy between molecules C and D and between molecules H and G (averaged). (b) Adjacent molecules C and D projected on the (c, b) plane. (c) Time series of the interaction energy between the molecules A and B and between molecules E and F (averaged). (d) Adjacent molecules A and B projected on the (c, b) plane. The cholesterol pairs shown, form chains along the c-axis in the crystal, that is, . . . ABAB . . . and . . . CDCD . . . The molecules in these chains have favorable interaction energies that arise mainly from the ring—ring interaction of adjacent molecules.

800 K MD in Vacuo *of Cholesterol, Ergosterol, and Lanosterol*

It has been shown that the chiral conformation of biologically important sterols is essential for their *in vivo* function.[46] Therefore, it is important that the sterols should preserve their stereochemistry during an MD simulation. In previous MD simulation studies of cholesterol in bilayers with other force fields, an inversion of the asymmetrical centers were observed.[47] To ensure that the chirality of the molecule is maintained and to test the new parameter set, we performed 2-ns MD simulations of the isolated cholesterol, ergosterol, and lanosterol molecules at 800 K, following the same protocol as in the crystal MD simulation. Although the temperature was elevated during the simulation, the stereochemistry of all the seven asymmetrical centers was preserved in all three sterols. To assess the stability of the steroid ring *in vacuo* and to estimate the role of the crystal environment in confering rigidity to the steroid nucleus, the torsional angles of the steroid ring from this simulation were monitored. The values and the standard deviations of these torsional angles (summarized in Table 13) are slightly larger than the ones obtained from the crystal simulation. However, they remain small, indicating that the rigidity is indeed inherent to the steroid ring and is not conferred by the crystal environment. In contrast to the steroid ring, and as expected, the flexible hydrocarbon tails underwent numerous *trans–gauche* transitions.

Supplementary Material

1. CHARMM parameter files: chol_par.inp, erg_par.inp and lan_par.inp include all the newly introduced parameters for cholesterol, ergosterol, and lanosterol, respectively in CHARMM27 format.
2. CHARMM topology files: cholesterol.rtf, ergosterol.rtf, lanosterol.rtf, NP.rtf, 4methylpent2ene.rtf, 3isopropyl2methylhex2ene.rtf, and 2.2dimethylcyclohexanol.rtf are the topology files for all the studied molecules.
3. Supplementary figures.

Conclusions

In this article, we present a parameter set for cholesterol, ergosterol, and lanosterol for the all-atom CHARMM27 molecular mechanics force field. The method used here for force-field determination is particularly useful for deriving parameters for rigid molecules, for which the flexibility is determined principally by vibrations, as is the case for these sterols. Furthermore, special care was taken to reproduce the rotational barrier of the hydroxyl around the O–C_3 bond. Fitting of the molecular mechanics potential onto that derived by quantum chemistry produced a good match both for cholesterol/ergosterol and lanosterol. Energy

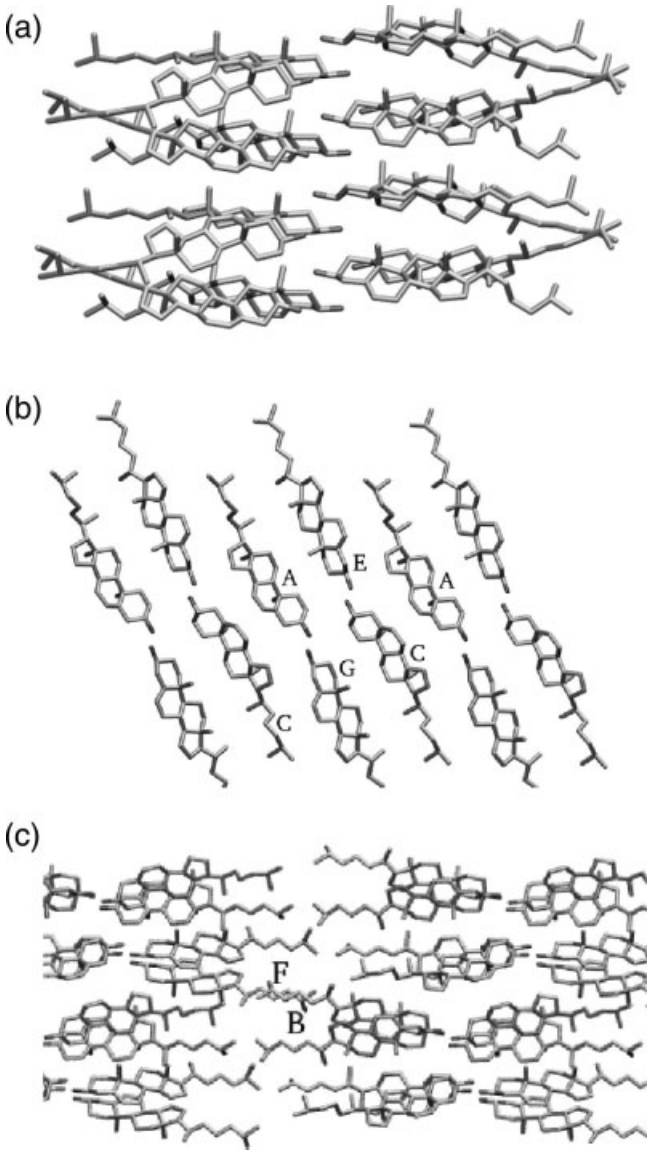

Figure 9. (a) Two-unit cells, projected on the (*c*, *b*) plane. The interactions that dominate in this direction is the hydrogen-bonded network and the van der Waals interactions between molecules on top of each other. (b) Three-unit cells, projected on the (*b*, *a*) plane. For clarity, only one of the layers of the crystal is presented. When constructing the crystal lattice, the corresponding transformations place the ring of molecule C next to the hydrogen-bonded molecules A and G of the next unit cell. The ring of molecule A is then placed next to the hydrogen-bonded molecules C and E of the neighboring unit cell. The van der Waals interactions between these molecules are favorable. (c) Part of the cholesterol crystal, projected on the (*a*, *b*) plane. The hydrocarbon chains of molecules B and F from neighboring unit cells come into close contact.

minimization and molecular dynamics of the X-ray structure of cholesterol lead to cell dimensions being reproduced within 2.4% of experimental values. The characteristic structural features of the crystal such as the rigidity of the sterol ring and the hydrogen-bonded network of the crystal were also reproduced. The nature of the nonbonded interactions in the cholesterol crystal were investigated by calculating the interaction energies between cholesterol molecules in the crystal. The favorable energy contributions arise mainly from van der Waals interactions between neighboring molecules, with a smaller contribution from the dynamically stable hydrogen-bonded network. A simulation of the three sterols at 800 K *in vacuo,* showed that the stereochemistry of all asymmetrical centers was preserved.

Sterols represent essential constituents of the lipid systems of all organisms. These 3β-hydroxy steroids, with different types of side chains, different numbers, and positions of C═C double bonds, and varying stereochemical characteristics, are crystalline, neutral, unsaponifiable alcohols with high melting points, and exhibit very similar physical and chemical properties. The force field presented herein may also be useful in simulating systems of other sterols or steroids, such as the phytosterols sigmasterol and sitosterol and many classes of steroids.

Deriving force field parameters for cholesterol is an essential step towards reliable and realistic simulations of sterol-containing membranes. Subsequent use of MD simulation will provide insights into the dynamical effects of sterols in membranes and help to derive biologically relevant structure–function relationships from a dynamical standpoint.

Acknowledgments

We thank Dr. A. C. Vaiana and Dr. S. Fischer for fruitful discussions. The calculations were performed on the HELICS, IWR–Universität Heidelberg (HBFG funds, hww cooperation).

References

1. Finegold, L. Cholesterol in Membrane Models; CRC Press: Boca Barton, FL, 1985.
2. Russell, D. W.; Setschell, K. D. Biochemistry 1992, 31, 4737.
3. Schoonjans, K.; Brendel, C.; Mangelsdorf, D.; Anxwerx, J. Biochim Biophys Acta 2000, 1529, 114.
4. Kusumi, A.; Tsuda, M.; Akino, T.; Ohnishi, O.; Terayama, Y. Biochemistry 1983, 22, 1165.
5. Bloch, K. In Biochemistry of Lipids and Membranes; Vance, J. E.; Vance, D. E., Eds.; Benjamin/Cummins Pub. Co. Inc.: New York, 1985, p. 1.
6. Simons, K.; Toomre, D. Nat Rev Mol Cell Biol 2000, 1, 31.
7. Haines, T. H. Prog Lipid Res 2001, 40, 299.
8. Risley, J. M. J Chem Ed 2002, 79, 377.
9. Smondyrev, A.; Berkowitz, M. L. Biophys J 2001, 80, 1649.
10. Murari, R.; Murari, M.; Baumann, W. J. Biochemistry 1986, 25, 1062.
11. Vist, M. R.; Davis, J. H. Biochemistry 1990, 29, 451.
12. Zuckermann, M. J.; Ipsen, J. H.; Mouritsen, O. G. Theoretical Studies of the Phase Behavior of Lipid Bilayers Containing Cholesterol; CRC Press: Boca Barton, FL, 1993, p. 223.
13. Miao, L.; Nielsen, M.; Thewalt, J.; Ipsen, J. H.; Bloom, M.; Zuckermann, M. J.; Mouritsen, O. G. Biophys J 2002, 82, 1429.
14. Baudry, J.; Tajkhorshid, E.; Molnar, F.; Phillips, J.; Schulten, K. J Phys Chem B 2001, 105, 905.
15. Mihailescu, D.; Smith, J. C. Biophys J 2000, 79, 1718.

16. Berneche, S.; Nina, M.; Roux, B. Biophys J 1998, 75, 1603.
17. Forrest, L.; Kukol, A.; Arkin, I.; Tielman, A.; Sansom, M. Biophys J 2000, 78, 55.
18. Smondyrev, A. M.; Berkowitz, M. L. Biophys J 1999, 77, 2075.
19. Chiu, S. W.; Jacobsson, E.; Scott, H. L. Biophys J 2001, 80, 1104.
20. Tu, K.; Klein, M. L.; Tobias, D. J. Biophys J 1998, 75, 2147.
21. Brooks, B. R.; Bruccoleri, R.; Olafson, B. D.; States, D. J.; Swaminathan, S.; Karplus, M. Comput Chem 1983, 4, 187.
22. Maple, J. R.; Hwang, M. J.; Stockfisch, T. P.; Dinur, U.; Waldman, M.; Ewig, C. S.; Hagler, A. T. J Comput Chem 1994, 15, 162.
23. Hagler, A. T.; Huler, E.; Lifson, S. J Am Chem Soc 1974, 96, 5319.
24. Liang, C.; Yan, L.; Hill, J. R.; Ewig, C. S.; Stouch, T. R.; Hagler, A. T. J Comput Chem 1995, 16, 883.
25. van Gunsteren, W. F.; Billeter, S. R.; Eising, A. A.; Hünenberger, P. H.; Krüger, P.; Mark, A. E.; Scott, W. R. P.; Tironi, I. G. Biomolecular Simulation: The GROMOS96 Manual and User Guide; Hochschuleverlag AG an der ETH Zürich: Zürich, Switzerland, 1996.
26. Baran, M.; Mazerski, J.; J Comp Chem 1995, 16, 883.
27. Shieh, H. S.; Hoard, L. G.; Nordman, C. E. Acta Crystallogr 1981, B37, 1538.
28. Weber, H. P.; Craven, B. M.; Sawzik, P. Acta Crystallogr 1991, B47, 116.
29. Shieh, H. S.; Hoard, L. G.; Nordman, C. E. Acta Crystallogr 1982, B38, 2411.
30. Pasenkiewicz–Gierula, M.; Rog, T.; Kitamura, K.; Kusumi, A. Biophys J 2000, 78, 1376.
31. Cournia, Z.; Vaiana, A. C.; Smith, J. C.; Ullmann, G. M. Pure Appl Chem 2004, 76, 189.
32. Vaiana, A. C.; Schulz, A.; Worfrum, J.; Sauer, M.; Smith, J. C. J Comp Chem 2003, 24, 632.
33. Vaiana, A. C.; Cournia, Z.; Costescu, I. B.; Smith, J. C. Comput Phys Commun 2005, 167, 34.
34. Harrison, R. J.; Nichols, J. A.; Straatsma, T. P.; Dupuis, M.; Bylaska, E. J.; Fann, G. I.; Windus, T. L.; Apra, E.; Anchell, J.; Bernholdt, D.; Borowski, P.; Clark, T.; Clerc, D.; Dachsel, H.; de Jong, B.; Deegan, M.; Dyall, K.; Elwood, D.; Fruchtl, H.; Glendenning, E.; Gutowski, M.; Hess, A.; Jaffe, J.; Johnson, B.; Ju, J.; Kendall, R.; Kobayashi, R.; Kutteh, R.; Lin, Z.; Littlefield, R.; Long, X.; Meng, B.; Nieplocha, J.; Niu, S.; Rosing, M.; Sandrone, G.; Stave, M.; Taylor, H.; Thomas, G.; van Lenthe, J.; Wolinski, K.; Wong, A.; Zhang, Z. A Computational Chemistry Package for Parallel Computers, Version 4.0.1; Pacific Northwest National Laboratory: Richland, WA, 2001.
35. Stevens, W. J.; Basch, H.; Krauss, M. J Chem Phys 1984, 81, 6026.
36. Scott, A. P.; Radom, L. J Phys Chem 1996, 100, 16502.
37. Breneman, C. N.; Wiberg, K. B. J Comp Chem 1990, 11, 361.
38. Cieplak, P.; Caldwell, J.; Kollman, P. J Comp Chem 2001, 22, 1048.
39. Feller, S. E.; Gawrisch, G.; MacKerell, A. D., Jr. J Am Chem Soc 2002, 124, 318.
40. Feller, S. E.; MacKerell, A. D., Jr. J Phys Chem B 2000, 104, 7510.
41. Yin, D.; MacKerell, A. D., Jr. J Comp Chem 1998, 19, 334.
42. Feller, S. E.; Yin, D.; Pastor, R. W.; MacKerell, A. D., Jr. Biophys J 1997, 73, 2269.
43. Schaftenaar, G.; Noordik, J. H. J Comput-Aided Mol Design 2000, 14, 123.
44. Shieh, H. S.; Hoard, L. G.; Nordman, C. E. Nature 1977, 267, 287.
45. Craven, B. M. Acta Crystallogr 1979, B35, 1123.
46. Crowder, C. M.; Westover, E. J.; Kumar, A. S.; Ostlund, R. E., Jr.; Covey, D. F. J Biol Chem 2001, 276, 44369.
47. Rog, T.; Pasenkiewicz–Gierula, M. Biophys J 2001, 81, 2190.